Similar land-form discovery: Complex absolute-value max pooling in complex-valued convolutional neural networks in interferometric synthetic aperture radar

Yuki Sunaga
Dept. Electrical Eng. & Info. Sys.
The University of Tokyo
Tokyo, Japan
sunaga_yuki@eis.t.u-tokyo.ac.jp

Ryo Natsuaki
Dept. Electrical Eng. & Info. Sys.
The University of Tokyo
Tokyo, Japan
natsuaki@ee.t.u-tokyo.ac.jp

Akira Hirose
Dept. Electrical Eng. & Info. Sys.
The University of Tokyo
Tokyo, Japan
ahirose@ee.t.u-tokyo.ac.jp

***Abstract*—In a complex-valued convolutional neural network, its elementary unit consists of a complex-valued convolution layer and a complex pooling layer. The pooling layer has a variety in its dynamics. In this paper, we propose complex absolute-value max pooling to extract complex-amplitude feature patterns meaningful for discovery and/or adaptive classification of land form in interferometric synthetic aperture radar (InSAR). Experimental examination into amplitude and phase values in convolutional kernels reveals that useful land-shape features emerge through self-organization in high-magnitude kernels, which suggests that the proposed dynamics is successful in extracting important features.**

***Index Terms*—Complex-valued neural network, interferometric synthetic aperture radar (InSAR), earth artificial intelligence (AI)**

I. Introduction

Many ideas have been proposed in these years to discover and/or classify adaptively local features in earth observation data [1]–[11]. They form the earth artificial intelligence (Earth AI) field. There, complex-valued convolutional neural networks are very useful for dealing with complex-amplitude local features consistently in interferometric synthetic aperture radar (InSAR) [12], [13]. In the near future earth AI systems, they will discover and continuously monitor specific land forms such as volcanos, floodable regions and glacier areas, which is significantly important for disaster prevention/reduction, global warming monitoring, and various other human life security. Related big-data processing frameworks have also been investigated widely and intensively [14], [15].

There are a variety of possible dynamics in a complex-valued elementary pair of a convolutional layer and pooling layer [16]–[19]. In particular, we have to design a pooling layer by considering what kind of features we need to extract, examining its available forward processing dynamics and learning algorithms.

A part of this work was supported by JSPS KAKENHI Grant Number 18H04105, and also by the Cooperative Research Project Program of the Research Institute of Electrical Communication (RIEC), Tohoku University. The Advanced Land Observing Satellite (ALOS) original data are copyrighted by Japan Aerospace Exploration Agency (JAXA) and provided under JAXA Fourth ALOS Research Announcement PI No. 1154 (AH).

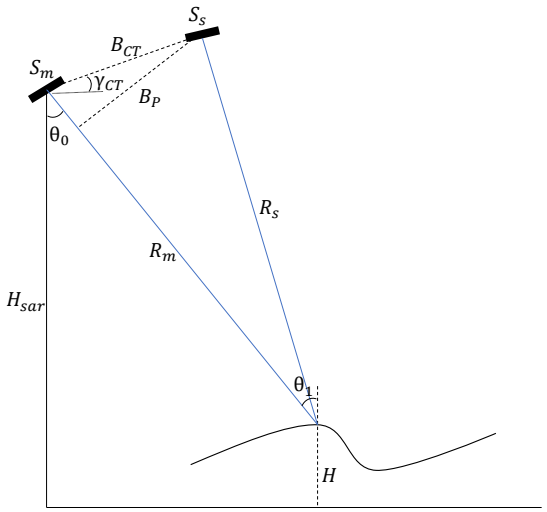

Fig. 1. Geometry of earth-surface height observation in interferometric synthetic aperture radar (InSAR).

In this paper, we propose complex absolute-value max pooling in the complex-valued convolutional neural networks to enhance the convolution signal-to-noise ratios by paying more attention to strong backscatterers and resulting convolutional outputs. Experiments demonstrate that this pooling realizes the self-organization of meaningful information in the convolutional kernels based on the assumption that high-intensity convolutional outputs originating from strong backscattering convey more information of the local target area by suppressing thermal and other noise. We find that this dynamics fits the purpose to discover and/or classify land-form features in InSAR.

978-1-7281-6926-2/20/$31.00 ©2020 IEEE

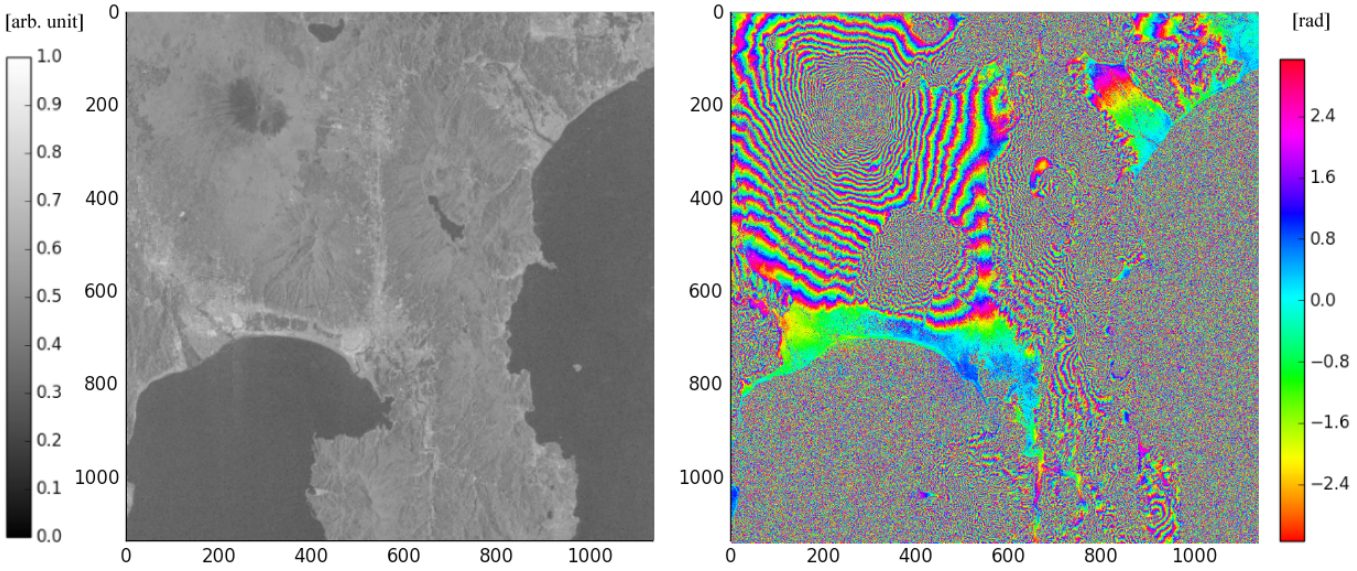

(a) (b)

Fig. 2. (a) Amplitude and (b) phase of InSAR interferogram [12].

II. Interferometric synthetic aperture radar observation

Fig. 1 shows rough geometry of interferometric earth observation by satellite-borne synthetic aperture radar (SAR) [20]. A SAR system illuminates the earth with an electromagnetic wave having a wavelength of λ, and receives backscattered wave as the amplitude and phase, i.e., complex-amplitude. With the observation data at two satellite positions $\mathrm{S_m}$ and $\mathrm{S_s}$, corresponding to master and slave observations, we can obtain an interferogram to calculate the land height changes ΔH by using their phase difference $\Delta\Phi$ as

$$\Delta H = \frac{\lambda R_{\mathrm{m}} \sin\theta}{4\pi B_{\mathrm{CT}} \cos(\theta - \gamma_{\mathrm{CT}})} \Delta\Phi \tag{1}$$

Then, we can make a height map by accumulating the phase changes pixel by pixel. This accumulation process is called "unwraping" since the phase value is "wrapped" into the range of $[-\pi, \pi)$. This calculated high-accuracy height map is called digital elevation model (DEM), which is obtained globally, spatially continuously and temporally frequently, and is very useful in human security.

Fig. 2 shows an (a) amplitude and (b) phase example of an InSAR interferogram obtained by Advanced Land Observing Satellite 2 (ALOS-2) of Japan Aerospace Exploration Agency (JAXA) for a Mt. Fuji area in Japan. The amplitude represents the magnitude of backscattering while the phase shows the height in a 2π-wrapped manner as expressed by (1). In this paper, we do not unwrap the phase image. Instead, we make spatial difference images in east-west and north-south directions so that we deal with land forms as slopes rather than its absolute height.

III. Proposed complex-valued convolutional neural network

Fig. 3 shows the construction of the complex-valued convolutional neural network we propose for learning and processing InSAR local data [12]. Complex-valued neural networks are suitable for processing complex-amplitude data including InSAR interferograms [21]–[27]. The two-direction difference images are fed to the network as two-channel inputs (C=2) and processed by one or more units of convolution and pooling layers. The image sizes and parameters are summarized as follows.

- Total data image size: ${}^0I \times {}^0J$ = 1,200×1,200 pixels
- Local window size: 28×28 pixels
- Convolution kernel number: K=9 for each channel, size: ${}^1p^{\mathrm{Conv}} \times {}^1q^{\mathrm{Conv}}$=27×27 pixels
- Pooling window size: ${}^1p^{\mathrm{Pool}} \times {}^1q^{\mathrm{Pool}}$=2×2 pixels

After a single or multiple convolution-and-pooling layer processing, we have a full connection layer to obtain total network outputs. In the present classification, we prepare the same number of output neurons as that of classes we intend.

A. Complex-valued convolution processing

In the following experiments, we feed the two complex-valued spatially-differential images mentioned above, denoted as ${}^{l=0}\boldsymbol{x}^{\mathrm{ew}}$ and ${}^{l=0}\boldsymbol{x}^{\mathrm{ns}}$ having common coordinates, to the neural network. A neural elementary unit is composed of a convolution layer and a pooling layer, and indexed by l in Fig. 3(a). Input terminal layer is labeled as $l = 0$, while the last layer is $l = L$, which is a fully connected network to work for decision.

We have single or multiple input signals (images) ${}^0\boldsymbol{x}^c$ generally, where c is the image label and 0 means the input

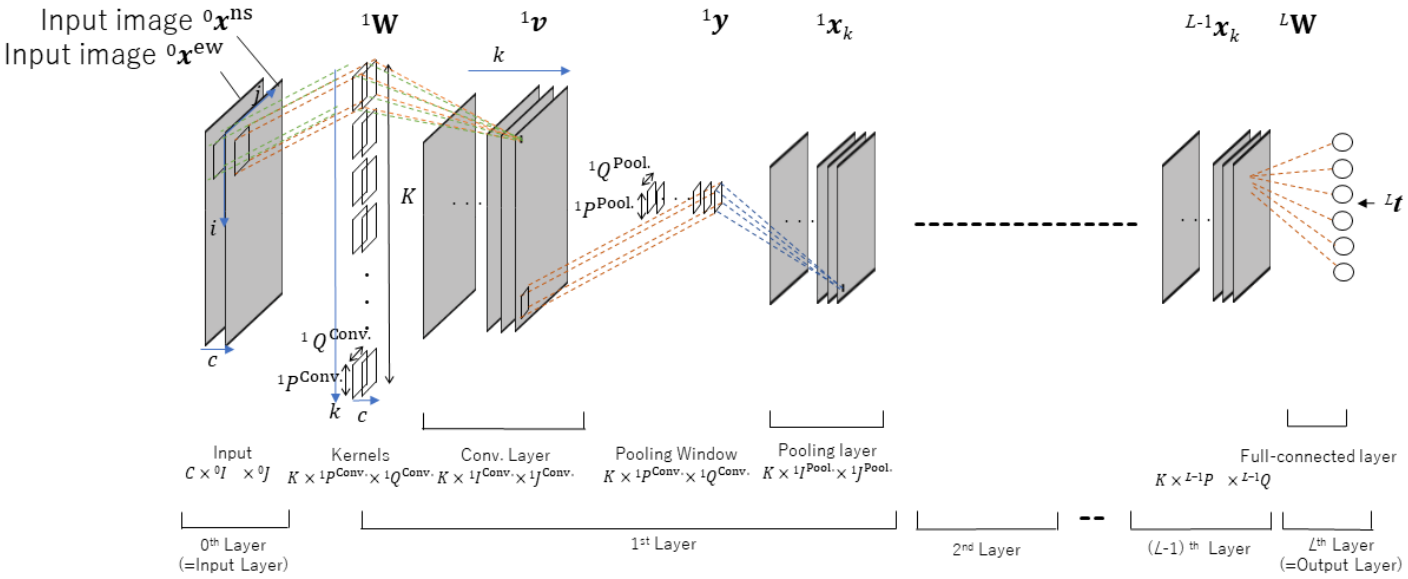

(a)

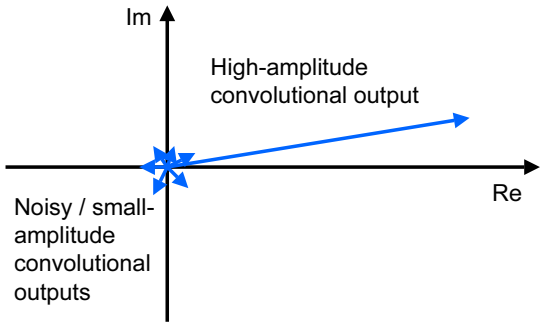

(b)

Fig. 3. (a) Construction of the convolutional neural network [12] and (b) conceptual illustration of selecting high-amplitude convolutional output by ignoring noisy/small-amplitude convolutional outputs in the pooling layer.

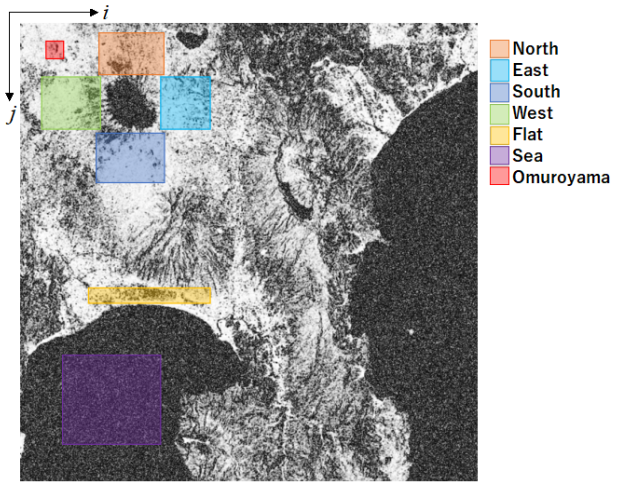

Fig. 4. Regions from which the teacher input images are clipped out. Orange: north, blue: east, dark blue: south, green: west, yellow: flat, purple: sea and red: Omuroyama [12].

layer. The output signal vector of the first convolution layer ${}^1\boldsymbol{v}_k = [{}^1v_{kij}]$ is expressed for input signal vectors ${}^0\boldsymbol{x}^c = [{}^0x^c_{i+p\ j+q}]$ as

$$ {}^1\boldsymbol{v} = f({}^1\boldsymbol{u}) \tag{2} $$

$$ {}^1u_{kij} = \sum_{c=1}^{C}\sum_{p=1}^{{}^1P}\sum_{q=1}^{{}^1Q} {}^1w^c_{k\,p\,q} \ * \ {}^1x^c_{i+p\ j+q} \tag{3} $$

$$ f({}^1u_{kij}) = \tanh(|{}^1u_{kij}|)\exp\left(j\arg({}^1u_{kij})\right) \tag{4} $$

where ${}^1\mathbf{W} = w^c_{k\,p\,q}$ is the neural weight connecting an input signal at position (p,q) in image c and a neuron at position (p,q) in convolutional kernel k in the first layer, and C, ${}^1P$ and ${}^1Q$ are the numbers of the total input channels, kernel vertical size and kernel horizontal size, respectively, $f(\cdot)$ is the activation function, and ${}^l\boldsymbol{u}$ is internal state of l-th layer neuron.

B. Forward processing and teacher-signal-backpropagation learning dynamics

We determine the neural dynamics as follows. The $(l-1)$-th layer output signals ${}^{l-1}\boldsymbol{x}$ are processed in l-th layer to generate

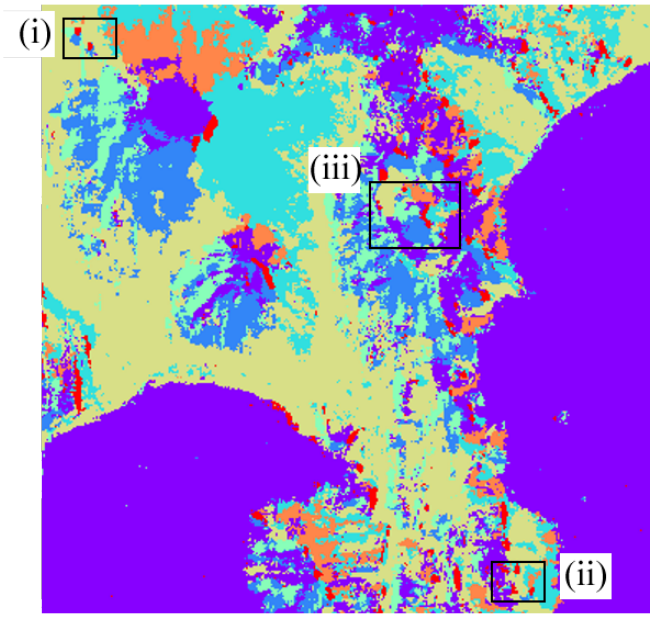

Fig. 5. Classification result obtained by the proposed complex-valued convolutional neural network.

${}^l\boldsymbol{x}$ as

$$
\begin{aligned}
{}^l\boldsymbol{x} &= f({}^l\boldsymbol{u}) && (5)\\
{}^l\boldsymbol{u} &= {}^l\mathbf{W}\ {}^{l-1}\boldsymbol{x} && (6)\\
f({}^l u_m) &= \tanh(|{}^l u_m|)\exp\left(j\arg({}^l u_m)\right) && (7)
\end{aligned}
$$

where ${}^l\mathbf{W} = [{}^l w_{nm}]$ is the connection weight between $m\ (= iJ + j)$-th neuron in $(l-1)$-th layer and $n\ (= pQ + q)$-th neuron in l-th layer.

We also determine the backpropagation dynamics of teacher signals, instead of errors, to update connection weights for supervised learning as follows. We calculate teacher signal vectors of each layers ${}^l\boldsymbol{t}$ backwards from the output layer. The teacher signal of $(l-1)$-th layer ${}^{l-1}\boldsymbol{t}$ is obtained from the teacher signal of l-th layer ${}^l\boldsymbol{t}$ as [26]

$$
{}^{l-1}\boldsymbol{t} = \left(f\left({}^l\boldsymbol{t}^*\ {}^l\mathbf{W}\right)\right)^* \tag{8}
$$

Then, we upadte ${}^l\mathbf{W}$ by using ${}^l\boldsymbol{t}$ as [28]–[30]

$$
\begin{aligned}
|{}^l w_{nm}| \leftarrow\ & |{}^l w_{nm}|\\
& - \epsilon^{\mathrm{a}}\{(1-|{}^l x_n^2|)(|{}^l x_n| - |{}^l t_n|\cos(\arg{}^l x_n - \arg{}^l t_n))|{}^{l-1}x_m|\cos{}^l\theta_{nm}^{\mathrm{rot}}\\
& - |{}^l x_n||{}^l t_n|\sin(\arg{}^l x_n - \arg{}^l t_n)\frac{|{}^{l-1}x_m|}{|{}^l u_n|}\sin{}^l\theta_{nm}^{\mathrm{rot}}\}
\end{aligned} \tag{9}
$$

$$
\begin{aligned}
\arg({}^l w_{nm}) \leftarrow\ & \arg({}^l w_{nm})\\
& - \epsilon^{\mathrm{p}}\{(1-|{}^l x_n^2|)(|{}^l x_n| - |{}^l t_n|\cos(\arg{}^l x_n - \arg{}^l t_n))|{}^{l-1}x_m|\sin{}^l\theta_{nm}^{\mathrm{rot}}\\
& + |{}^l x_n||{}^l t_n|\sin(\arg{}^l x_n - \arg{}^l t_n)\frac{|{}^{l-1}x_m|}{|{}^l u_n|}\cos{}^l\theta_{nm}^{\mathrm{rot}}\}
\end{aligned} \tag{10}
$$

$$
{}^l\theta_{nm}^{\mathrm{rot}} = \arg({}^l x_n) - \arg({}^{l-1}x_m) - \arg({}^l w_{nm}) \tag{11}
$$

where ϵ^{a} and ϵ^{p} are learning rates of amplitude and phase respectively.

C. Complex absolute-value max pooling

The output of the pooling layer is invariant for small position changes in the output patterns of the former layer. In other words, a pooling layer absorbs small position changes and small rotations of input images. Here, we determine the complex-valued pooling process as

$$
{}^l y_{k\,i\,j} = {}^l v_{k\ \underset{p,q}{\operatorname{argmax}}\,|{}^l v_{k\,p\,q}|} \tag{12}
$$

That is, the output of a pooling layer is a value that has maximum norm in the pooling window. If the local pattern in the input image is similar to the complex-amplitude pattern in a kernel of a convolutional layer, the norm of the output signal becomes large, and then the following pooling layer extracts this signal. At the same time, as shown in Fig. 3(b), this process enhances high-amplitude signals in the convolution process, resulting in extraction of phase information in high-amplitude input signals. This treatment reflects the thought that high-intensity signals are more meaningful, and should be extracted intensively than small or noise components.

Then we design the dynamics of the teacher-signal back-propagation in the pooling layer as follows. We make teacher signals backpropagate in order to update only the neurons that pass the signals to the following layer. Specifically, we get teacher signals of the convolution layer ${}^l\hat{\boldsymbol{t}}$ from teacher signals for the pooling layer ${}^l\boldsymbol{t}$ as

$$
{}^l\hat{t}_{k\,p\,q} = \begin{cases} {}^l t_{k\,i\,j} & \text{if } {}^l y_{k\,i\,j} = {}^l v_{k\,p\,q} \\ {}^l v_{k\,p\,q} & \text{otherwise} \end{cases} \tag{13}
$$

D. Fully connected network for decision

For classification, the output layer of the complex-valued convolutional neural network is composed as a fully connected network, just like a usual complex-valued neural network. The input signal of the fully connected layer ${}^{L-1}\boldsymbol{x} = [{}^{L-1}x_n]$ is obtained from the preceding pooling layer as

$$
{}^{L-1}x_{\ k\times I\times J+i\times J+j} = {}^{L-1}\ y_{k\,i\,j} \tag{14}
$$

where $k \times I \times J + i \times J + j (= n)$ is represented one dimensionally when the size of the output image of the pooling layer has K images of $I \times J$ pixels.

IV. Experiments and Results

Fig. 4 presents seven teacher zones from which we cut out local teacher signals for seven classes (categories), namely, north-facing slope, east-facing slope, south-facing slope, west facing slope, flat plain, sea, and Omuroyama (scoria cone). Omuroyama is a Japanese word meaning small eruptive crater. By including Omuroyama as a class, we intend to find volcanos of a similar shape for disaster prediction/mitigation. In the following experiments, we used a convolutional network having a single pair of convolution and pooling layers. We determined the teacher signals used at the full-connection network as $[1\ \ -1\ \ -1\ \ -1\ \ -1\ \ -1\ \ -1]^{\mathrm{T}}$ for north-facing slope, $[-1\ 1\ \ -1\ \ -1\ \ -1\ \ -1\ \ -1]^{\mathrm{T}}$ for east-facing slope, and so on, where $[\cdots]^{\mathrm{T}}$ stands for transpose.

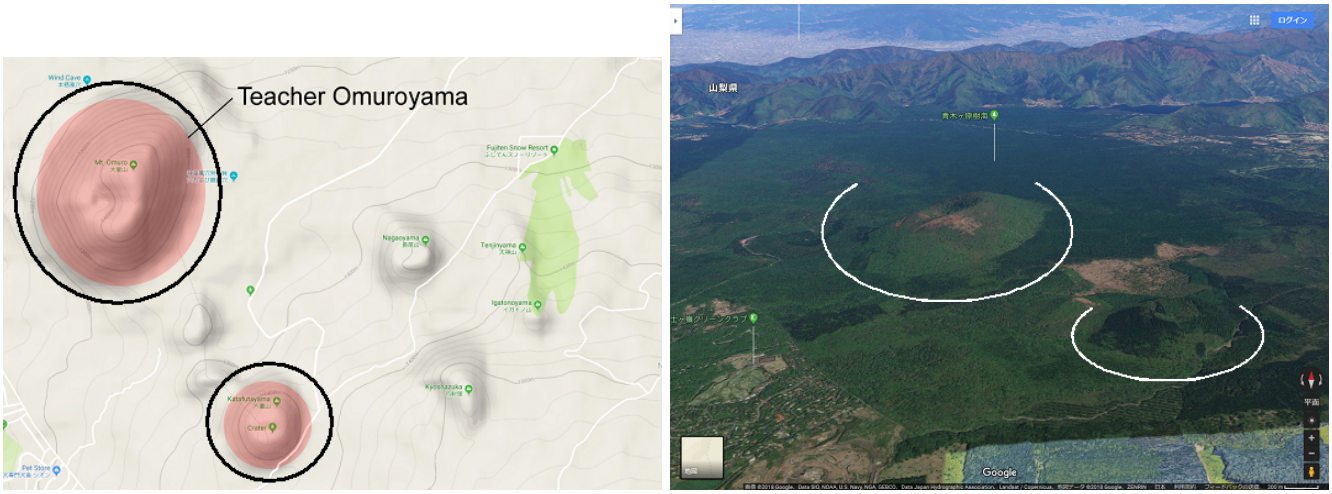

(a) (b)

Fig. 6. (a) Area (i) land shape map and (b) its bird's eye view (Google earth) including teacher Omuroyama and another Omuroyama-shaped mountain named Katafutayama.

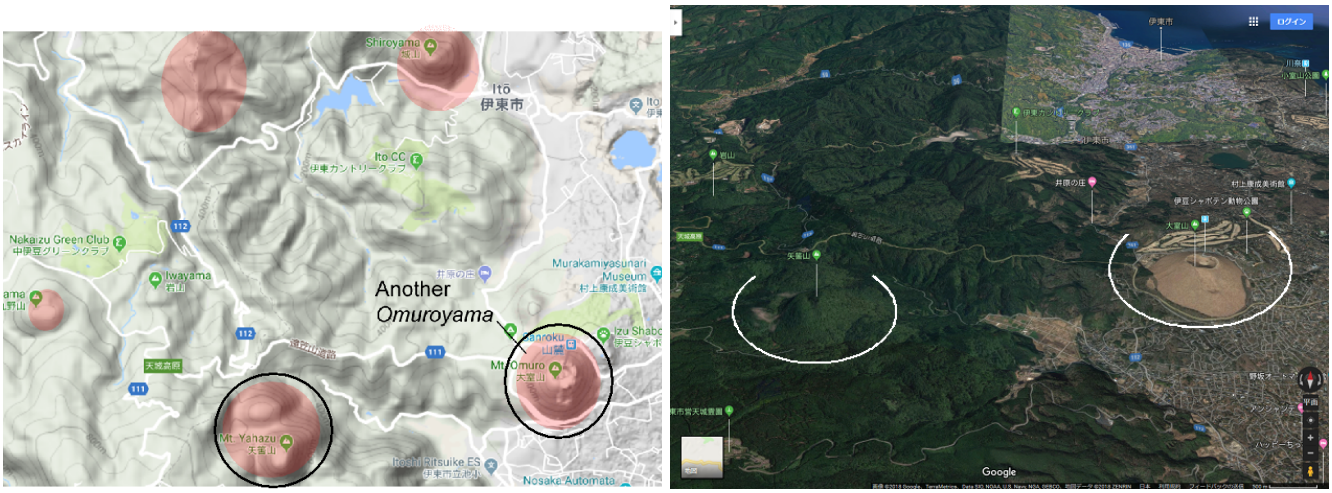

(a) (b)

Fig. 7. (a) Area (ii) land shape map and (b) its bird's eye view (Google earth) including another typical Omuroyama and similar mountain Yahazuyama.

Fig. 5 presents the classification result for the whole target region after the learning is completed. In this paper, we focus on the extraction of Omuroyama-like land form. In the figure, small red areas indicate the decision of Omuroyama shape. We can see that they are scattered widely.

Let's investigate into Areas (i), (ii) and (iii) in Fig. 5. Fig. 6(a) shows Area (i) with red patches at the Omuroyama decisions. Besides the teacher Omuroyama, we find another Omuroyama class patch in the east-south direction, which is an eruptive crater named Katafutayama. It is smaller in its size than the teacher Omuroyama, but we can see in the photo in Fig. 6(b) on the right-hand side that the shape is homothetic. That is, the complex-valued convolutoinal network succeeded in finding a similar land shape patch.

Fig. 7(a) shows the result for Area (ii), in which we find another Omuroyama. (The mountain is named also Omuroyama, and this is a typical Omuroyama in Japan in its shape.) In the photo in Fig. 7(b), we can confirm the similar shape. Another patch shows another mountain having similar land form.

Fig. 8(a) shows Area (iii), Hakone area, a popular sightseeing area located in the Fuji-Hakone National Park. The marked two mountains are "Futagoyama," meaning twin mountains. In Fig. 8(b), they are found surely to have also Omuroyama-like shapes. However, these mountains are much bigger than the teacher Omuroyama, in particular in its height. Since there are no high mountains around them, it is not widely known that these mountains have the Omuroyama-like shape. In this way, however, they are discovered as Omuroyama-class mountains surprisingly.

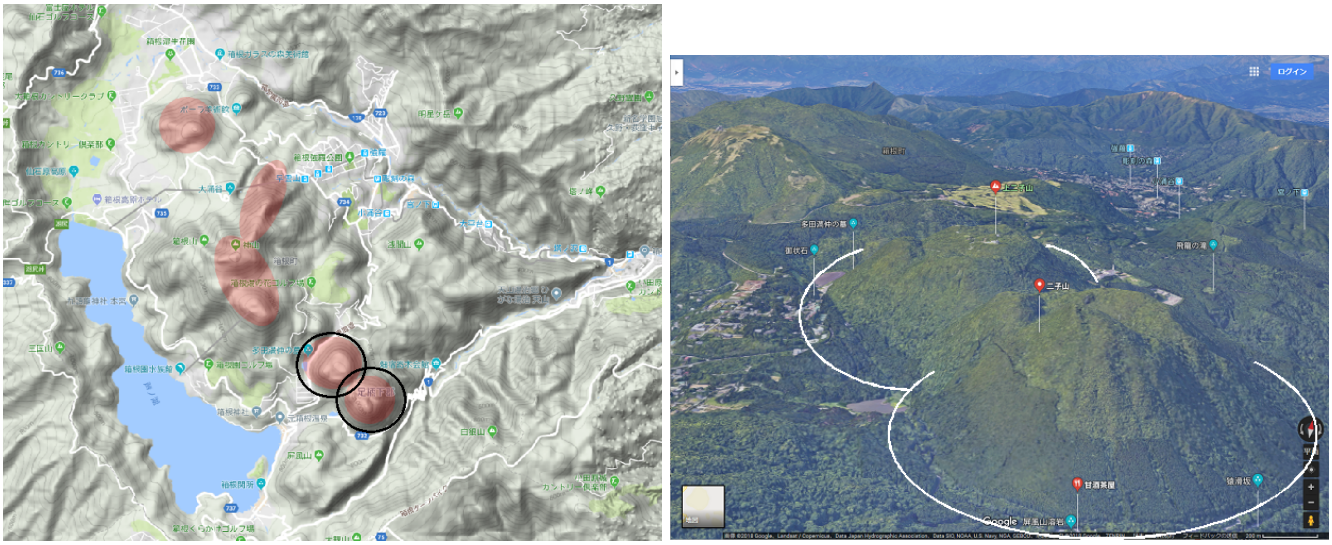

(a) (b)

Fig. 8. (a) Area (iii) land shape map and (b) its bird's eye view (Google earth) including another typical Omuroyama and similar mountains Futagoyama ("Twin Mountains").

V. Self-organized images in the convolutional kernels

Fig. 9 presents the convolution kernels before and after the learning process. They are found to self-organize to be meaningful kernels as follows. Gray-scale images show the amplitude values while color images represent phase values. The initial values before the learning is shown in Fig. 9(a). Both the amplitude and the phase are at random, presenting no specific features. In contrast, Fig. 9(b) presents the emerged kernels. Both in $\mathbf{W^{c=1}}$ and $\mathbf{W^{c=2}}$, the amplitude values are large in four kaernels, i.e., k = 1, 2, 6 and 9. Other kernels are relatively small. The large ones indicate significant meanings.

The kernel k=2 of $\mathbf{W^{c=1}}$ in Fig. 9(b) shows large values in the amplitude, and its phase values are pink in the left half while green in the right half. This spatial pattern represents an eastward up-and-down, that is, a ridge in the north-south direction. Similarly, Kernel k=9 in $\mathbf{W^{c=2}}$ also shows large amplitude values, and its phase has green values in the upper half while pink values in the lower half. It means a northward up-and-down, or a ridge in the east-west direction. In addition, the combination of these two features represents a mountain shape having a peak at around the center. In this way, the kernels self-organize into meaningful spatial information representation. The correspondence to the large amplitude reveals the successful feature extraction with the complex absolute-value max pooling in the complex domain.

VI. Summary

This paper proposed the complex absolute-value max pooling to extract land form features adaptively by dealing with local complex-amplitude in interferometric synthetic aperture radar. The network discovers and classifies adaptively special land forms such as Omuroyama. We confirmed in the experiment that meaningful features emerge in the kernels in the convolutional layers by investigating the complex-amplitude spatial patterns.

References

[1] D. Espinoza-Molina and M. Datcu, "Earth-observation image retrieval based on content, semantics, and metadata," *IEEE Transactions on Geoscience and Remote Sensing*, vol. 51, no. 11, pp. 5145–5159, 2013.

[2] F. Shang and A. Hirose, "Quaternion neural-network-based PolSAR land classification in poincare-sphere-parameter space," *IEEE Transactions on Geoscience and Remote Sensing*, vol. 52, no. 9, pp. 5693–5703, 2014.

[3] K. R. Kurte, U. M. Bhangale, S. S. Durbha, R. L. King, and N. H. Younan, "Accelerating big data processing chain in image information mining using a hybrid HPC approach," in *International Geoscience and Remote Sensing Symposium (IGARSS) 2016 Beijing*, 2016, pp. 7597–7600.

[4] U. M. Bhangale, K. R. Kurte, S. S. Durbha, R. L. King, and N. H. Younan, "Big data processing using HPC for remote sensing disaster data," in *International Geoscience and Remote Sensing Symposium (IGARSS) 2016 Beijing*, 2016, pp. 5894–5897.

[5] F. Shang and A. Hirose, "Averaged-Stokes-vector-based polarimetric SAR data interpretation," *IEEE Transactions on Geoscience and Remote Sensing*, vol. 53, no. 8, pp. 4536–4547, August 2015.

[6] H. Kim and A. Hirose, "Unsupervised fine land classification using quaternion auto-encoder-based polarization feature extraction and self-organizing mapping," *IEEE Transactions on Geoscience and Remote Sensing*, vol. 56, no. 3, pp. 1839–1851, March 2018.

[7] S. De, D. Ratha, D. Ratha, A. Bhattacharya, and S. Chaudhuri, "Tensorization of multifrequency PolSAR data for classification using an autoencoder network," *IEEE Geoscience and Remote Sensing Letters*, vol. 15, no. 4, pp. 542–546, April 2018.

[8] H. Kim and A. Hirose, "Polarization feature extraction using quaternion neural networks for flexible unsupervised PolSAR land classification," in *International Geoscience and Remote Sensing Symposium (IGARSS) 2018 Valencia*, no. TUP2.PD.3, July 2018.

[9] S. De, L. Bruzzone, A. Bhattacharya, F. Bovolo, and S. Chaudhuri, "A novel technique based on deep learning and a synthetic target datadata for classification of urban areas in PolSAR data," *IEEE Journal of Selected Topics in Applied Earth Observation*, vol. 11, no. 1, pp. 154–170, 2018.

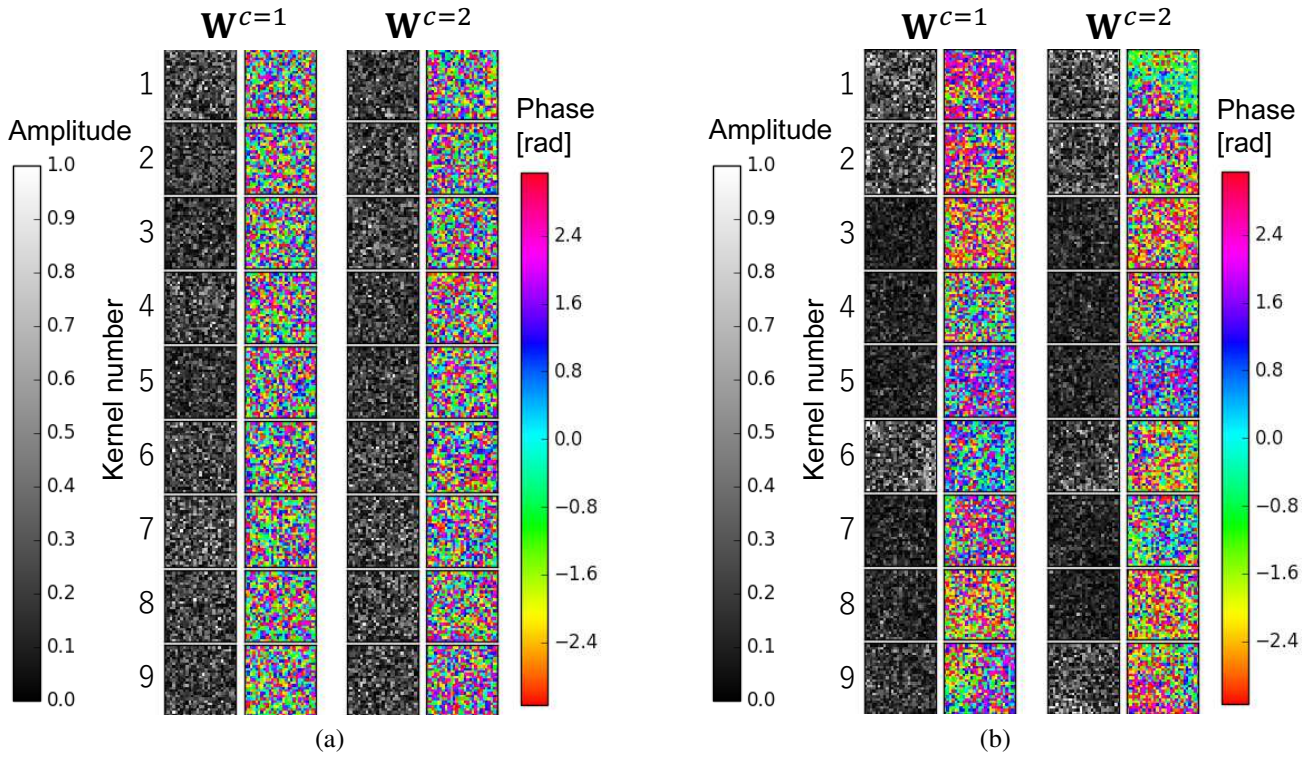

Fig. 9. Amplitude (gray) and phase (color) of convolutional weights for kernel number k (a) before and (b) after the learning process ($\mathbf{W^{c=1}}$ for east-west difference data, $\mathbf{W^{c=2}}$ for north-south difference data).

[10] H. Kim and A. Hirose, "Codebook-based hierarchical polarization feature for unsupervised fine land classification using high-resolution PolSAR data," in *International Geoscience and Remote Sensing Symposium (IGARSS) 2018 Valencia*, no. WEP1.PD.9, July 2018.

[11] ——, "Unsupervised hierarchical land classification using self-organizing feature codebook for decimeterresolution PolSAR," *IEEE Transactions on Geoscience and Remote Sensing*, vol. 57, no. 4, pp. 1894 – 1905, April 2019.

[12] Y. Sunaga, R. Natsuaki, and A. Hirose, "Land form classification and similar land-shape discovery by using complex-valued convolutional neural networks," *IEEE Transactions on Geoscience and Remote Sensing*, vol. 57, no. 10, pp. 7907–7917, October 2019.

[13] ——, "Proposal of complex-valued convolutional neural networks for similar land-shape discovery in interferometric synthetic aperture radar," in *International Conference on Neural Information Processing (ICONIP) 2018 Siep Reap*, December 2018, pp. 340–349.

[14] A. Hirose, S. Tsuda, and R. Natsuaki, "Structurization of synthetic aperture radar information by using neural networks," in *SAR in Big Data Era: Models, Methods and Applications (BIGSARDATA) 2017 Beijing*, 10.1109/BIGSARDATA.2017.8124936, November 2017, pp. 1–4.

[15] A. Hirose, Y. Sunaga, and R. Natsuaki, "Recent progress in adaptive SAR data structurization in complex and hypercomplex domain," in *International Workshop on Big SAR Data (BigSARData) 2019 Beijing*, August 2019, pp. 1–6.

[16] Z. Zhang, H. Wang, F. Xu, and Y.-Q. Jin, "Complex-valued convolutional neural network and its application in polarimetric SAR image classification," *IEEE Transactions on Geoscience and Remote Sensing*, vol. 55, no. 12, pp. 7177–7188, December 2017.

[17] M. Tygert, J. Bruna, S. Chintala, Y. LeCun, S. Piantino, and A. Szlam, "A mathematical motivation for complex-valued convolutional networks," *Neural Computation*, vol. 28, pp. 815–825, 2016.

[18] T. Nitta, *Complex-Valued Neural Networks: Utilizing High-Dimensional Parameters*, T. Nitta, Ed. Pennsylvania: Information Science Reference, 2009.

[19] A. Hirose (Ed.), *Complex-Valued Neural Networks: Advances and Applications*, ser. IEEE Press Series on Computational Intelligence. New Jersey, U.S.A.: IEEE Press and Wiley, April 2013.

[20] R. Natsuaki and A. Hirose, *Local, fine co-registration of SAR interferometry using the number of singular points for the evaluation*. In-Tech, March 2012, vol. Interferometry / Book 1, 95-110, ISBN 979-953-307-376-6.

[21] A. Hirose and S. Yoshida, "Generalization characteristics of complex-valued feedforward neural networks in relation to signal coherence," *IEEE Transactions on Neural Networks and Learning Systems*, vol. 23, pp. 541–551, 2012.

[22] R. Natsuaki and A. Hirose, "Circular property of complex-valued correlation learning in CMRF-based filtering for synthetic aperture radar interferometry," *Neurocomputing*, vol. 134, pp. 165–172, 2014.

[23] A. Hirose and R. Eckmiller, "Behavior control of coherent-type neural networks by carrier-frequency modulation," *IEEE Transactions on Neural Networks*, vol. 7, pp. 1032–1034, 1996.

[24] ——, "Coherent optical neural networks that have optical-frequency-controlled behavior and generalization ability in the frequency domain," *Applied Optics*, vol. 35, no. 5, pp. 836–843, 1996.

[25] R. Natsuaki and A. Hirose, "Phase property in complex-correlation and real-imaginary-correlation filtered SAR interferograms and its influence on DEM quality," in *Proceedings of Asia-Pacific Conference on Synthetic Aperture Radar (APSAR) 2013 Tsukuba*, September 2013, pp. 218–221.

[26] A. Hirose, "Applications of complex-valued neural networks to coherent optical computing using phase-sensitive detection scheme," *Information Sciences –Applications–*, vol. 2, pp. 103–117, 1994.

[27] ——, *Complex-Valued Neural Networks, 2nd Edition*. Heidelberg, Berlin, New York: Springer, 2012.

[28] ——, "Continuous complex-valued back-propagation learning," *Electronics Letters*, vol. 28, no. 20, pp. 1854–1855, 1992.

[29] A. Hirose and R. Eckmiller, "Behavior control of coherent-type neural networks by carrier-frequency modulation," *IEEE Transactions on Neural Networks*, vol. 7, no. 4, pp. 1032–1034, 1996.

[30] K. Oyama and A. Hirose, "Adaptive phase-singular-unit restoration with entire-spectrum-processing complex-valued neural networks in interferometric SAR," *Electronics Letters*, vol. 54, no. 1, pp. 43–45, January 2018.